
Cryptic diversity within the *Gonyaulax spinifera* species complex, its relation to the cyst- defined species *Spiniferites bentorii*, *S. mirabilis* and *S. membranaceus*, with the description of *Gonyaulax carbonell- mooreae* sp. nov. (Gonyaulacales, Dinophyceae)

Huang Shuning ¹, Mertens Kenneth ², Nguyen-ngoc Lam ^{3,*}, Doan-nhu Hai ³, Krock Bernd ⁴, Li Zhun ⁵,
Luong Doc Quang ⁶, Billien Gwenael ², Pospelova Vera ⁷, Shin Hyeon Ho ⁸, Plewe Sascha ⁹,
Gu Haifeng ^{1,*}

¹ Third Institute of Oceanography, Ministry of Natural Resources Xiamen, China

² Ifremer Littoral Concarneau, France

³ Institute of Oceanography, Vietnam Academy of Science and Technology Nha Trang, Viet Nam

⁴ Department of Ecological Chemistry Alfred Wegener Institute-Helmholtz Center for Polar and Marine Research Bremerhaven, Germany

⁵ Biological Resource Center/Korean Collection for Type Cultures (KCTC), Korea Research Institute of Bioscience and Biotechnology Jeongseup, Korea

⁶ Faculty of Biology University of Sciences, Hue University Hue City, Viet Nam

⁷ Department of Earth and Environmental Sciences University of Minnesota Minneapolis Minnesota, USA

⁸ Division of Fisheries Life Sciences Pukyong National University Busan, Republic of Korea

⁹ Leibniz-Institut für Ostseeforschung Warnemünde Rostock, Germany

* Corresponding authors : Lam Nguyen-ngoc, email address : ngoclam-ion@planktonviet.org.vn ;
Haifeng Gu, email address : guhaifeng@tio.org.cn

Abstract :

The fossil dinoflagellates *Spiniferites bentorii*, *S. mirabilis*, and *S. membranaceus* are known to inhabit recent sediments and are often used to reconstruct past sea-surface conditions. However, information on their corresponding motile cells has been rare. We isolated single cysts resembling these fossil species from China and France to yield *Gonyaulax spinifera*-like cells. *Gonyaulax* strains were also established from Viet Nam and South Korea by isolating single cells. Both cysts and cells were examined by light and scanning electron microscopy, and their LSU rRNA genes were sequenced. A new *Gonyaulax* species, *G. carbonell-mooreae*, was obtained from *S. bentorii*-like cysts and considered the equivalent of *Spiniferites bullatus*, dating back to the Campanian. *Gonyaulax kunsanensis* was related to *S. mirabilis*-like cysts. A typical *S. membranaceus* cyst from France yielded cells resembling *G. lewisiae* but shared only 75% similarity in LSU rRNA gene sequence with those from South Korea. Molecular phylogeny revealed that the pronounced apical boss is systematically significant, whereas the presence of intergonal processes is insignificant. Two ASVs of 18S rRNA V4 region were respectively identified as *G. kunsanensis* and *G. lewisiae* from the Tara Oceans metabarcoding data. *Gonyaulax kunsanensis* has a

wide distribution in the Pacific, Indian, and Atlantic Oceans, but *G. lewisiae* has a restricted distribution. One strain of *G. kunsanensis* was examined for yessotoxin content using liquid chromatography coupled with tandem mass spectrometry (LC–MS/MS), but no detectable amounts of toxins were observed. Our results uncover the hidden diversity within the *G. spinifera* species complex and stress the significance of cyst morphology in the taxonomy of *Gonyaulax*.

Keywords : cyst, dinoflagellate, *Gonyaulax*, *Spiniferites bullatus*, Tara Oceans, yessotoxin

Abbreviations: BI, Bayesian inference; BS, bootstrap support; GTR, general time-reversible; ITS, internal transcribe spacer; LC-MS/MS, liquid chromatography coupled with tandem mass spectrometry; LM, light microscopy; LSU, large subunit; MCMC, Markov chain Monte Carlo; ML, maximum likelihood; NCBI, National Center for Biotechnology Information; OTU, operational taxonomic unit; PP, posterior probabilities; RAxML, Randomized Axelerated Maximum Likelihood; SEM, Scanning electron microscopy; YTX, yessotoxin;

1. Introduction

Dual nomenclature is sanctioned for dinoflagellates species with both a fossil type (generally a cyst; Head et al. 2023) and an equivalent extant type (usually a vegetative cell) under the International Code of Nomenclature for algae, fungi and plants (ICN) (Art. 11.1, Turland et al. 2018). An exceptional example of dual nomenclature is found in the fossil genus *Spiniferites* and its related extant genus *Gonyaulax*. Cysts of *Spiniferites* are characterized by a tabulation formula of 2pr, 4', 6'', 6c, 5–6s, 6''', 1p, 1''''', gonal and/or intergonal processes, sutural ridges or septa connecting their bases, and a precingular archeopyle formed by the loss of plate 3'' (Mertens and Carbonell-Moore 2018). It was Wall (1965) who first related *Spiniferites* to *Gonyaulax* through the incubation of *Spiniferites bentorii*-like cysts. Since then, a dozen *Spiniferites* species have been germinated to yield different *Gonyaulax* species (e.g. Lewis et al. 1999, Ellegaard et al. 2003, Mertens et al. 2015, Gu et al. 2024). The *Gonyaulax spinifera* complex corresponds to *G. spinifera*, *G.*

digitale and *G. diegensis*, three species that are difficult to discriminate and form part of the "spinifera group" of Kofoed (1911) (Mertens and Carbonell-Moore 2018).

Gonyaulax spinifera like cells with two antapical spines were assigned to *G.*

pospelovana and *G. montresoriae* recently based on the *Spiniferites* like cysts they produced (Gu et al. 2024, Huang et al. 2025).

More than one hundred *Spiniferites* species have been described (Williams et al. 2017), but only around ten of them are known to be living (Marret et al. 2020). Key features for differentiating *Spiniferites* species include the size and shape of the central body, the shape of gonial processes, the presence or absence of intergonal processes and an apical boss, wall surface ornamentation, and cingular displacement (Mertens et al. 2018). However, morphological differences among species are often subtle and may require careful examination with the aid of scanning electron microscopy for differentiation.

The diversity of living *Spiniferites* species might have been greatly underestimated. For instance, two new *Spiniferites* species similar to *S. delicatus* have been reported recently. One of them, *S. pseudodelicatus*, has occasional intergonal processes compared to the exclusively gonial processes found in *S. delicatus* (Gu et al. 2022). Another was reported as cysts of *Gonyaulax pospelovana* but not formally described with a fossil type, differing from *S. pseudodelicatus* only in the lack of an apical boss and an archeopyle that is not reduced (Gu et al. 2024). All these species share a petaloid gonial process, distinguishing them from other *Spiniferites* species, whose processes are not wide (Mertens et al. 2018). *Spiniferites delicatus* was

originally described from a temperate British estuary (Reid 1974), but later was reported in subtropical to tropical coastal regions (Zonneveld et al. 2013). Whether specimens from warmer waters are indeed *S. delicatus* remains unclear.

Spiniferites membranaceus and *S. bentorii* have been considered easy to identify and thought to have a wide, temperate to tropical distribution (Zonneveld et al. 2013). The former has exclusively gonal processes and a large flange connecting two antapical processes, while the latter is pear-shaped with a pronounced apical boss. *Spiniferites membranaceus* was originally described from Pleistocene or Holocene deposits of the Ashkelon borehole on the coastal plain of Israel (Rossignol 1964). The cyst-theca relationship was established by incubating cysts collected nearby England and Ireland, and the equivalent motile cells were described as *Gonyaulax membranacea* (Lewis et al. 1999, Ellegaard et al. 2003), but later renamed as *G. lewisiae* (Head et al. 2024). *Spiniferites mirabilis* is similar to *S. membranaceus* in terms of an antapical flange but differs in having consistent intergonal processes (Rossignol 1964). The corresponding *Gonyaulax* species has not been described yet.

Spiniferites bentorii was described from Quaternary sediments from the Ashdod borehole on the coastal plain of Israel (as *Hystriosphera bentori*) (Rossignol 1964). *Spiniferites bentorii*-like cysts from the Adriatic Sea germinated to yield a new *Gonyaulax* species described as *G. nezaniae*; several other *Spiniferites bentorii*-like cysts from the Bohai Sea, which exhibit intergonal processes, share 98% similarity in LSU rRNA gene sequence with *G. nezaniae* (Gu et al. 2021).

One of interesting feature on *Gonyaulax* is that some species are able to produce yessotoxin (YTX), Homo-YTX and their derivatives (Rhodes et al. 2006, Riccardi et al. 2009, Álvarez et al. 2016, Huang et al. 2025), including a putative *G. lewisiae* (Pitcher et al. 2019). However, the number of *Gonyaulax* subject to YTX analysis is still limited.

Spiniferites membranaceus and *S. bentorii* have been associated with estuarine habitats (Debenay et al. 2003), but the latter has also been regarded as an indicator of high salinity (34–36) (Harland et al. 2006), suggesting several ecotypes or even hidden species are present. To better understand the diversity of living *Spiniferites*, we isolated cysts resembling *S. membranaceus*, *S. mirabilis* and *S. bentorii* and performed germination experiments. Both cyst and theca morphologies were examined in detail with light microscopy and scanning electron microscopy, and molecular phylogeny was inferred based on LSU sequences. In addition, a strain of *Gonyaulax* was examined for yessotoxin production by liquid chromatography coupled with tandem mass spectrometry (LC-MS/MS).

2. Material and methods

2.1. Sample collection and treatment

Sediment samples were collected along the coast of China from 2016 to 2022 using an Ekman grab sampler (Table 1). Sediment from the top 2 centimeters was gathered and stored in the dark at 4 °C. Approximately 5 g of wet sediment was mixed with 20 mL of sterile-filtered seawater and vigorously stirred to disperse it. The mixture was

sequentially passed through 125 μm and 10 μm sieves, and the cyst mixture collected on the 10 μm sieve was further extracted following Bolch (1997). Single cysts were isolated and transferred into 96-well cell culture plates containing f/2-Si culture medium (Ryther and Guillard 1962) for germination. The culture conditions were set at 20 °C with a light intensity of 90 $\mu\text{mol m}^{-2}\text{s}^{-1}$ under a 12-hour light and 12-hour dark cycle (referred to as standard culture conditions). Emergent cells were observed using an inverted Eclipse TS100 microscope (Nikon, Tokyo, Japan) and strains were established (Table 1). Some of these strains generated cysts in culture spontaneously. Phytoplankton samples were collected in Hue, Viet Nam and Jeju Island, South Korea (water temperature: 21 °C) using a plankton net (20 μm -mesh). Single cells were isolated and using the inverted Eclipse TS100 microscope with a micropipette to establish strains (Table 1).

2.2. Light microscopy (LM)

An Axiocam HRc digital camera (Zeiss Axiocam HRc) was used with an Axiocam Imager optical microscope (Zeiss, Göttingen, Germany) to observe and capture images of cysts and motile cells. The sizes of cysts and vegetative cells were measured on the captured images. The cells were stained with a 1:100,000 dilution of SYBR Green (Sigma Aldrich) and their nuclear shape, position, and chloroplast distribution within the cells were observed and documented using the Zeiss-38 filter set (excitation BP 470/40, beam splitter FT 495, emission BP 525/50) on the optical microscope.

2.3. Scanning electron microscopy (SEM)

For SEM observations, 2 mL of mid-exponential batch cultures of strains TIO219, TIO902 and TIO1221, or isolated cysts, were fixed by Lugol's Iodine solution (4% final concentration) at room temperature and then rinsed by centrifugation with deionized water. After rinsing, samples were dehydrated, critical point dried, and examined following standard protocols (Gu et al. 2021). The stub of VINIF07 finally gold coated in a Polaron E5100 sputter coater and then were examined on Merlin-Compact VP Scanning Electron Microscope (Zeiss, Germany) at the Leibniz Institute of Institute of Baltic Sea Research, Warnemünde, Rostock, Germany. Plate labeling follows the Kofoidian system (Kofoid 1911), except for sulcal plate labeling which follows Carbonell-Moore et al. (2022). The term 'apical boss' refers to a pronounced protrusion in the apex of cysts as opposed to 'apical pore' in the apex of cells (Wall 1965).

2.4. PCR amplifications and sequencing

Single cells were isolated and washed several times with sterile distilled water. They were lysed by applying gentle force on the coverslip using an inverted microscope and then pipetted into a PCR tube for templates. Various regions of rRNA genes including the partial LSU (D1–D6) and ITS1–5.8S–ITS2, were amplified using primer pairs specified previously, following standard protocols (Gu et al. 2021). The newly obtained sequences were deposited in GenBank with accession numbers (Table 1).

2.5. Sequence alignment and phylogenetic analyses

The newly obtained LSU rRNA gene sequences were compared with those of

Gonyaulax species and related taxa in NCBI. The MAFFT v7.110 (Kato and Standley 2013) online program (<http://mafft.cbrc.jp/alignment/server/>) was used for sequence alignment with default settings and checked manually using BioEdit v7.0.5 (Hall 1999). Maximum likelihood (ML) analysis was performed using raxmlGUI 1.5 (Silvestro and Michalak 2012) with the GTR+G model with 1,000 bootstrap replicates (using the ‘ML + rapid bootstrap’ option). For Bayesian inference (BI), the program jModelTest (Posada 2008) was used to select the most appropriate model of molecular evolution based on the Akaike Information Criterion (AIC). Bayesian reconstruction of the data matrix was performed using MrBayes 3.2 (Ronquist and Huelsenbeck 2003) and the best-fitting alternative model, GTR+G, was adopted. The four Markov chain Monte Carlo (MCMC) chains ran for 5,000,000 generations, sampling once every 1,000 generations. The first 10% of burn-in trees were discarded. To examine the posterior probability (PP) of each clade, the consensus tree of majority rule was established.

2.6. Yessotoxin analysis

Cultures of strain TIO1274 were grown in 200 mL Erlenmeyer flasks under standard culture conditions. At stationary phase, determined via linear regression of log-transformed cell count time series, approximately 4.8×10^5 cells were concentrated with a Universal 320 R centrifuge at $850 \times g$ for 10 min at room temperature. Algal pellets were transferred to 2 mL microcentrifuge tubes and stored at -20°C until analysis for the quantification of intracellular YTX. Measurements were carried out by liquid chromatography (LC 1100, Agilent, Waldbronn Germany) coupled to tandem mass spectrometry (API 4000 QTrap, Sciex, Darmstadt Germany), as detailed

in Wang et al. (2019). In brief, separation was performed on a reversed phase column with gradient elution from a 40% aqueous methanol–acetonitrile mixture to 100% methanol–acetonitrile. Yessotoxin and 23 of its structural variants (Table S1) were screened in negative mode by selected reaction monitoring (SRM).

2.7. *The biogeography of Gonyaulax kunsanensis and G. lewisiae based on the Tara Oceans 18S V4 metabarcoding data*

The complete 18S rRNA gene sequences of *Gonyaulax kunsanensis* (OR145345, Shin et al. 2024) and *G. lewisiae* (AF022155, Saunders et al. 1997) were submitted to <https://oba.mio.osupytheas.fr>. A homologous metabarcode sequence (18S V4) exactly matching *Gonyaulax kunsanensis* and *G. lewisiae* was obtained respectively. The biogeography of the corresponding OTU was displayed on a world map, and covariation with environmental variables (temperatures, salinity, distance to coast, latitude) was analyzed online (Vernette et al. 2021).

3. Results

Gonyaulax carbonell-mooreae sp. nov. H.Gu, Lam Nguyen-Ngoc & K.N.Mertens

Description:

Cells were 52–57 µm long and 42–60 µm wide with two short antapical spines. The epitheca was conical with a distinct shoulder on the right. The cell surface was thick and heavily reticulated. The cingulum descended about its width without an overhang. Cells exhibited a plate formula of 2pr, 4', 6'', 6c, 5s, *6''', 2p, 1'''''. A ventral pore was present at the junction of plates 4'a and 4'p. Cysts of *G. carbonell-mooreae* were oval,

55–70 μm long and 43–66 μm wide, with a pronounced apical boss. Cysts had a smooth to granular surface, with gonal and one or two intergonal processes. The processes measured 5–16 μm in length. The archeopyle was not reduced, corresponding to plate 3''.

Holotype (designated here): SEM stub of thecate cells from a culture established from a cell isolated from Viet Nam, shown in Fig. 2 and stored at the Oceanographic Museum, Institute of Oceanography, Nha Trang, Viet Nam, with the accession number VMO 202401.

Type locality: Hue, Viet Nam (16°33'11"N, 107°38'47"E).

Habitat: Marine and planktonic with benthic cyst stage.

Etymology: The epithet "*carbonell-mooreae*" honors Consuelo Carbonell-Moore, who performed pioneering work on dinoflagellate taxonomy.

GenBank accession numbers: ITS1-5.8S-ITS2: PQ423724 (VINIF07) and PQ423725 (VINIF08); LSU rRNA gene: PQ423728 (VINIF07) and PQ423729 (VINIF08)

3.1. Morphology of *Gonyaulax carbonell-mooreae*

Cysts of *Gonyaulax carbonell-mooreae* from China were oval, measuring 55.0–70.2 μm ($62.2 \pm 7.7 \mu\text{m}$, $n=3$) in length and 43.0–65.7 μm ($52.9 \pm 11.6 \mu\text{m}$, $n=3$) in width, with a pronounced apical boss (Fig. 1a). The outer surface was smooth to microgranular. Both gonal and one or two intergonal processes were present (Fig. 1b, c, e). The processes of cysts from Xiamen Bay were 11.5–15.7 μm in length (Fig. 1d, f), whereas those from the Bohai Sea were 4.5–6.0 μm in length. The gonal processes were usually trifurcated with bifid terminations, while the intergonal processes were bifurcated (Fig.

1d). The paracingulum descended with a displacement of its width without overhang (Fig. 1c). The precingular archeopyle was not reduced and corresponded to plate 3'' (Fig. 1d). ITS sequence of isolate TIO717 from Xiamen Bay was identical to those of cells from Viet Nam (strains VINIF07 and VINIF08).

Cells of *Gonyaulax carbonell-mooreae* from Viet Nam measured 51.8–57.1 μm ($54.1 \pm 2.7 \mu\text{m}$, $n=3$) in length, 42.3–60.0 μm ($50.2 \pm 6.4 \mu\text{m}$, $n=9$) in width, with two antapical spines measuring 4.2–5.4 μm in length. Cells of *G. carbonell-mooreae* from Xiamen Bay were dark brown and ornamented with a thick reticulation (Fig. S1).

Cells of *G. carbonell-mooreae* exhibited the plate formula 2pr, 4', 6'', 6c, 5s, *6''', 2p, 1'''''. The thecae displayed a sexiform gonyaulacoid tabulation (Fensome et al. 1993, text-fig. 64) with an S-type ventral organization (Fensome et al. 1993, text-figs 82B, D) and neutral torsion (Fensome et al. 1993, text-fig. 83B). The cingulum descended about its width without an overhang (Fig. 2a).

Plate 1' was narrow and elongated, connected to the apical pore complex (apc), and plate 4' was divided into 4'a and 4'p, with the ventral pore located between them (Fig. 2c). The plates were heavily reticulated, with a trichocyst pore in each reticulation (Fig. 2b, c). Plates 2' and 3' were large and similar in size. Six precingular plates were present, with the sixth (6'') being triangular and smaller (Fig. 2b, d). The apc comprised a pore plate with a lenticular pore inside, surrounded by raised ridges of neighbouring plates (Fig. 2e). The cingulum consisted of six cingular plates (Fig. 2f). Plate 1p was much smaller than plate 2p (Fig. 2g). The sulcus was composed of the anterior sulcal

plate (Sa), anterior left sulcal plate (Ssa), posterior left sulcal plate (Ssp), right anterior sulcal plate (Sda), and right posterior sulcal plate (Sdp) (Fig. 2h, i). A schematic drawing of the tabulation is provided in Fig. 3.

3.2. Morphology of *Gonyaulax kunsanensis*

Cysts of *Gonyaulax kunsanensis* were spherical, with a diameter of 31.8–37.5 μm ($34.2 \pm 1.9 \mu\text{m}$, $n=6$) (Fig. 4a). The cyst surface ranged from smooth to granular. Both gonal and one to three intergonal processes were present (Fig. 4b, c, e). The processes measured 6.5–10.8 μm in length ($8.7 \pm 1.4 \mu\text{m}$, $n=18$), with perforations at the base (Fig. 4d, f). The gonal processes were usually trifurcated with bifid terminations, whereas the intergonal processes were bifurcated (Fig. 4d). A membranous flange, approximately 12.5 μm long, displayed four processes at the antapex. The paracingulum descended with a displacement of 1.5 times its width without overhang (Fig. 4c). The archeopyle was reduced, corresponding to plate 3'' (Fig. 4d).

Cells of *G. kunsanensis* were 25.6–36.6 μm ($31.4 \pm 2.8 \mu\text{m}$, $n=23$) long and 21.6–31.3 μm ($25.2 \pm 2.6 \mu\text{m}$, $n=23$) wide. The cells had a conical epitheca and a truncated hypotheca, with a pronounced apical horn (Fig. 5a). Leaf-like chloroplast lobes were scattered on the cell surface (Fig. 5b). The nucleus was elongated and located in the hypocone (Fig. 5c). The cingulum was positioned in the middle and descended about two times its width, with an overhang of 0.75 times its width (Fig. 5d). Two equal antapical spines were generally present, approximately 3.0 μm long (Fig. 5a, d).

Cells of *G. kunsanensis* had a plate formula of 2pr, 4', 6'', 6c, 5s, *6''', 2p, 1'''' (Fig. 5d–i). Plates 1' and 4' were narrow and elongated, while plates 2' and 3' were large and similar in size (Fig. 5g). Plate 6'' was triangular and smaller than the others (Fig. 5e, f). The apc consisted of a pore plate with a lenticular pore inside, surrounded by raised ridges of the neighbouring plates (Fig. 5g). Plate 1p was much smaller than plate 2p (Fig. 5g). The sulcus was composed of plates Sa, Ssa, Ssp, Sda, and Sdp (Fig. 5i).

3.3. *Morphology of Gonyaulax cf. lewisiae*

The central body of the cyst of isolate 18-652 from coastal waters of Brittany in northwestern France was spherical, with a diameter of 40.0 μm (Fig. 6a). The processes were exclusively gonal, 9.7–12.9 μm in length with trifurcate tips. The paracingulum descended 2.5 times its width (Fig. 6c). A pronounced antapical flange was 17.7 μm in height (Fig. 6a, d). The archeopyle was reduced (Fig. 6b).

The germinated cell was 41.2 μm long, 35.0 μm wide. It had a conical epitheca and a rounded hypotheca without antapical spines (Fig. 6e). The cingulum descended 3.0 times its width, with an overhang of 2.0 times its width (Fig. 6f, g).

3.4 *Molecular phylogeny*

Gonyaulax carbonell-mooreae strains TIO717 (Xiamen Bay, East China Sea), HSN128 (the Bohai Sea) and VINIF07 (Viet Nam coast, the South China Sea) differed from each other at only one position in LSU sequences. Strain TIO717 shared 79.34% similarity with a *G. nezaniae* strain from the Adriatic Sea (GenBank accession:

MW775690), and 81.50% similarity with a putative *G. nezaniae* from the Bohai Sea (GenBank accession: MW775691). *Gonyaulax kunsanensis* strains shared identical LSU sequences with a strain from South Korea (GenBank accession: OR149166). *Gonyaulax lewisiae* strains from South Korea shared identical LSU sequences with *G. lewisiae* (GenBank accession: AY154965), but only shared 75.46% similarity with *Gonyaulax* cf. *lewisiae* isolate 18-652 from France.

Phylogenetic trees using maximum likelihood (ML) and Bayesian inference (BI) based on LSU sequences had similar topologies. The ML tree showed five well-resolved clades, corresponding to the families Ceratiaceae, Protoceratiaceae, Pyrophacaceae, Gonyaulacaceae, and Lingulodiniaceae (Fig. 7). Gonyaulacaceae was monophyletic with maximal support (ML BS: 100; BI PP: 1.0), comprising two clades (clade I and clade II). *Gonyaulax carbonell-mooreae* formed a sister clade with *G. nezaniae* from the Adriatic Sea and the Bohai Sea, with maximal support. *Gonyaulax* cf. *lewisiae* was a sister of *Spiniferites lazus* and *G. lewisiae* with maximal support, and these formed a sister clade to *G. kunsanensis* with maximal support. All these strains fell within Clade I of Gonyaulacaceae.

3.5 Yessotoxin

Gonyaulax kunsanensis strain TIO1274 from Xiamen Bay was studied for the presence of 24 YTXs (Table S1), but none of these were detected above the detection limit of 33.8 fg cell⁻¹ expressed as YTX equivalents.

3.6 Biogeography and ecology of *Gonyaulax kunsanensis* and *G. lewisiae* based on Tara Oceans metabarcoding data

ASV71086 from the Tara Oceans 18S V4 metabarcoding data was identical to the sequence of *Gonyaulax kunsanensis*. ASV71086 was widely distributed, with a maximum relative abundance of 1.91×10^{-3} (Fig. 8). It was mostly found in subsurface water samples, with maximum abundances detected at temperatures of 10–30°C (Fig. S2).

ASV76747 from the Tara Oceans 18S V4 metabarcoding data had 99.7% similarity to the sequence of *Gonyaulax lewisiae*. ASV76747 was only found at a station on the west coast of the USA, with a maximum relative abundance of 1.19×10^{-3} (Fig. S3), where the temperature was around 19.5°C (Fig. S4).

4. Discussion

The hidden diversity within the *Spiniferites bentorii*, *S. mirabilis* and *S. membranaceus* species complex was uncovered for the first time through a careful examination of both cyst and theca morphology, aided by molecular sequences. Additionally, the systematic significance of the apical boss and intergonal processes

was further elucidated.

4.1 *Spiniferites bentorii* like cysts

Spiniferites bentorii is characterized by a pronounced apical boss, occasional intergonal processes, and microgranulate surface (Rossignol 1964, Limoges et al. 2018). Cysts of *Gonyaulax carbonell-mooreae* differ from *S. bentorii* in their consistent intergonal processes and smooth walls (Table 2). Cysts of *G. carbonell-mooreae* resemble *S. bullatus* in terms of a pronounced apical protuberance, smooth wall and two intergonal processes, which is a fossil species dating back to Campanian (Beilstein 1994). *Spiniferites bentorii* with intergonal processes appears genetically very close to those with exclusively gonal processes in terms of LSU sequences, but cell morphology from the former type has not been examined yet (Gu et al. 2021). A similar morphological variability was observed in *S. mirabilis* subsp. *mirabilis* and *S. mirabilis* subsp. *serratus* although morphology and molecular sequences from the corresponding motile cells is not available (Van Nieuwenhove et al. 2018).

Spiniferites bentorii-like cysts with consistent intergonal processes give rise to *G. carbonell-mooreae* here, in addition to *G. nezaniae*, as previously reported (Gu et al. 2021). Two pronounced antapical processes were observed in the cyst of *G. nezaniae*, but not in those of *G. carbonell-mooreae*. *Spiniferites bentorii* from Buzzards Bay, Massachusetts, USA, does not exhibit pronounced antapical processes (Pospelova et al. 2005); thus, these are possibly cysts of *G. carbonell-mooreae*.

The sympatric occurrence of *G. carbonell-mooreae* and *G. nezaniae* in the Bohai Sea (Gu et al. 2021) suggests that previous reports on the abundance of *S. bentorii* in

China (Wang et al. 2004) might be overestimated. On the other hand, we failed to detect *G. nezaniae* in the Tara Oceans metabarcoding data (Gu personal observations) although *S. bentorii* was reported to have a wide distribution (Zonneveld et al. 2013). However, it is worth noting that the Tara Oceans data is from a single sampling, so it might miss species that are not present throughout the year. At present, 18S rDNA sequences of *G. carbonell-mooreae* are not available, thus their distribution cannot be explored using these molecular data. A sediment trap study at eight sites worldwide in estuarine, coastal and offshore environments reveal that *S. bentorii* was only abundant in the temperate Saanich Inlet of Canadian Pacific (Pospelova et al. 2018), but there is a possibility it was primarily *Spiniferites ramosus* with a pronounced apical boss (see Plate 1, Figure 6 in Price and Pospelova 2011). Our findings of *G. carbonell-mooreae* in subtropical and tropical waters suggest that the wide distribution of *S. bentorii* as previously reported by Zonneveld et al. (2013) might be too broad.

Gonyaulax carbonell-mooreae is characterized by a pronounced apical horn, heavy reticulations and two antapical spines of equal size; thus, it may be classified within the *G. spinifera* species complex (Kofoid 1911). However, *G. carbonell-mooreae* can be distinguished from *G. spinifera* by the absence of cingulum overhang and from other closely related species in a smaller cingular displacement (1.0 versus 2.0 or greater) (Table 3). *Gonyaulax carbonell-mooreae* is similar to *G. diegensis* which also lacks cingulum overhang, and they share polygonal reticulations, but the latter is usually longer than 75 μm (Kofoid 1911) whereas the former is less than 60 μm .

4.2 Spiniferites membranaceus like cysts

Cysts of *Gonyaulax kunsanensis* are similar to *Spiniferites membranaceus*, but can be distinguished by the presence of intergonal processes, and occasional perforations at the base of the processes. Another difference is the number of processes in the antapical flange, which is four in the former but only two in the latter (Table 2). *Spiniferites membranaceus* was originally described from the Pleistocene-Holocene sediments from the coastal plain of Israel (Rossignol 1964), found off the British Isles (Reid 1974), in the North Atlantic Ocean and adjacent seas (Harland 1983), and along the coast of New South Wales of Australia (McMinn, 1991), although Wall et al. (1977) and Harland (1983) stated that *S. membranaceus* sensu Reid (1974) is probably not conspecific with that of Rossignol (1964). It was also reported in the Sea of Japan (Orlova et al. 2004), but their figure 21 show a cyst lacking an antapical flange, thus indicating a misidentification. *Spiniferites membranaceus* has also been reported from South Korea (Pospelova and Kim 2010) and is confirmed here by molecular sequencing of several strains of *G. lewisiae* from Jeju Island. The water temperature is around 21 °C when *G. lewisiae* strains were collected in South Korea, thus is consistent with the Tara Oceans metabarcoding data when this species occurred (19.5 °C). A presumable *S. membranaceus* (isolate 18-652) from France yielded a cell without antapical spines, but the cingular displacement and overhang fit the description of *G. lewisiae* (Lewis et al. 1999).

Cysts of *G. kunsanensis* are also similar to *S. mirabilis*. *Spiniferites mirabilis* was originally described from Pleistocene or Holocene sediments from the coastal plain of Israel (Rossignol 1964), and is characterized by an antapical flange with five to seven

processes, resembling the fingers of a glove (Limoges et al. 2018). *Spiniferites mirabilis* has been reported widely, e.g. in the Western Atlantic Ocean (Wall and Dale 1966), in estuarine waters of the Atlantic USA (Pospelova et al. 2005), North Atlantic Ocean (Harland 1983), New South Wales, Australia (McMinn 1991), the Baltic Sea (Head 2007), the Gulf of Mexico (Limoges et al. 2013), South Korea (Pospelova and Kim 2010), West Japan (Matsuoka 1985), and the northeastern Pacific Ocean (Pospelova et al. 2008).

Spiniferites mirabilis from the Sea of Japan is probably a cyst of *Gonyaulax kunsanensis*, as only four processes are observed in the antapical flange (fig. 24) (Orlova et al. 2004). Similarly, *S. mirabilis* from the Yellow Sea is likely a cyst of *G. kunsanensis* as well (figure 3G) (Liu et al. 2012). *Spiniferites mirabilis* was proposed to include two subspecies, subsp. *mirabilis* and subsp. *serratus*, but currently, only sequences from the former are available (Gu et al. 2021). Therefore, morphological and molecular information from many more germinated cells are needed to understand the variability of cyst morphology.

Gonyaulax kunsanensis from China fits the original descriptions (Shin et al. 2024), and our findings of this species along the coast of China suggest it is a widespread species. This can be further confirmed by the Tara Oceans metabarcoding data, which shows its presence in the Indian Ocean and Atlantic Ocean as well (Fig. 8). The failure to detect YTX in a strain of *G. kunsanensis* is not surprising, as the majority of *Gonyaulax* species are nontoxic (Gu et al. 2024). YTX production has been implicated in *G. lewisiae* from South Africa (Pitcher et al. 2019), but to date, YTX has not been

reported in a cultured strain of *G. lewisiae*.

4.3 Molecular phylogeny

Our molecular phylogeny is consistent with previous results, supporting the monophyly of *Gonyaulax* (Gu et al. 2022, Shin et al. 2024). The presence of two pronounced antapical processes appears meaningful, as *S. membranaceus*, *S. lazus*, and cysts of *G. kunsanensis* group together. On the other hand, the presence of intergonal processes is systematically insignificant above species level since cysts of *G. kunsanensis* bear such processes, whereas *S. lazus* and *S. membranaceus* have exclusively gonal processes. This is also supported by the clustering of *S. bentorii* with and without intergonal processes (Gu et al. 2021). Additionally, the presence of an antapical flange is not significant above species level either, as *S. mirabilis* is separated from *S. membranaceus*.

The close relationship between *G. carbonell-mooreae* and *G. nezaniae* suggest that a pronounced apical boss is systematic important. An apical boss has also been reported in other *Spiniferites* species, such as *S. mirabilis* and *S. membranaceus* (Gurdebeke et al. 2018, Limoges et al. 2018) but it is not as well developed compared to that of *S. bentorii*. Only 75% similarity in LSU sequences was observed between our new *Gonyaulax* cf. *lewisiae* isolate and other *G. lewisiae* strains, suggesting that *S. membranaceus* like cysts might harbor cryptic diversity.

Assemblages of dinoflagellate cysts have been used to reconstruct sea-surface conditions based on the modern analogue technique (de Vernal et al. 2020). Understanding their modern distribution and related environments is crucial for such

analysis. Our findings of cryptic diversity within the *S. bentorii*, *S. mirabilis* and *S. membranaceus* complex provide challenges and new insight for such reconstructions.

Acknowledgements

This work was supported by the National Natural Science Foundation of China (42030404, 42076085), the Vingroup Innovation Foundation via Project VinIF.2022.DA00079 and the management of Marine Fishery Bio-Resources Center (2025) funded by the National Marine Biodiversity Institute of Korea (MABIK). KNM and GB were financially supported by the French National Research Agency (ANR) PhenoMap project, ANR-20-CE02-0025.

REFERENCES

- Álvarez, G., Uribe, E., Regueiro, J., Blanco, J. & Fraga, S. 2016. *Gonyaulax taylorii*, a new yessotoxins-producer dinoflagellate species from Chilean waters. *Harmful Algae* 58:8–15.
- Beilstein, U. 1994: Mikrofloren (Sporomorphen, Dinophyceen) aus der regressiven Oberkreide des Benue-Troges, Nigeria. *Geologisches Institut der Universität zu Köln, Sonderveröffentlichungen* 95:1–305.
- Bolch, C. 1997. The use of sodium polytungstate for the separation and concentration of living dinoflagellate cysts from marine sediments. *Phycologia* 36:472–78.
- Carbonell-Moore, M. C., Matsuoka, K. & Mertens, K. N. 2022. Gonyaulacalean

- tabulation revisited using plate homology and plate overlap, with emphasis on the ventral area (Dinophyceae). *Phycologia* 61:195–210.
- de Vernal, A., Radi, T., Zaragosi, S., Van Nieuwenhove, N., Rochon, A., Allan, E., De Schepper, S., Eynaud, F., Head, M.J., Limoges, A., Londeix, L., Marret, F., Matthiessen, J., Penaud, A., Pospelova, V., Price, A. & Richerol, T. 2020. Distribution of common modern dinoflagellate cyst taxa in surface sediments of the Northern Hemisphere in relation to environmental parameters: The new n=1968 database. *Mar. Micropaleontol.* 159:101796.
- Debenay, J., Carbonel, P., Morzadec-Kerfourn, M.-T., Cazaubon, A., Denèfle, M. & Lézine, A.M. 2003. Multi-bioindicator study of a small estuary in Vendee (France). *Estuar. Coast. Shelf Sci.* 58:843–60.
- Ellegaard, M., Daugbjerg, N., Rochon, A., Lewis, J. & Harding, I. 2003. Morphological and LSU rDNA sequence variation within the *Gonyaulax spinifera*-Spiniferites group (Dinophyceae) and proposal of *G. elongata* comb. nov. and *G. membranacea* comb. nov. *Phycologia* 42:151–64.
- Gu, H., Huo, K., Krock, B., Bilien, G., Pospelova, V., Li, Z., Carbonell-Moore, C., Morquecho, L., Ninčević, Ž. & Mertens, K. N. 2021. Cyst-theca relationships of *Spiniferites bentorii*, *S. hyperacanthus*, *S. ramosus*, *S. scabratus* and molecular phylogenetics of *Spiniferites* and *Tectatodinium* (Gonyaulacales, Dinophyceae). *Phycologia* 60:332–53.
- Gu, H., Mertens, K. N., Derrien, A., Bilien, G., Li, Z., Hess, P., Séchet, V., Krock, B., Amorim, A., Li, Z., Pospelova, V., Smith, K. F., MacKenzie, L., Yoon, J. Y.,

- Kim, H. J. & Shin, H. H. 2022. Unravelling the *Gonyaulax baltica* species complex: Cyst-theca relationship of *Impagidinium variaseptum*, *Spiniferites pseudodelicatus* sp. nov. and *S. ristingensis* (Gonyaulacaceae, Dinophyceae), with descriptions of *Gonyaulax bohaiensis* sp. nov, *G. amoyensis* sp. nov. and *G. portimonensis* sp. nov. *J. Phycol.* 58:465–86.
- Gu, H., Zheng, J., Huang, S., Morquecho, L., Krock, B., Shin, H. H., Li, Z., Derrien, A. & Mertens, K. N. 2024. A new dinoflagellate *Gonyaulax pospelovana* with resting cysts resembling *Spiniferites delicatus* and its biogeography and ecology revealed by DNA metabarcoding. *Phycologia* 63:74–88.
- Gurdebeke, P. R., Mertens, K. N., Bogus, K., Marret, F., Chomérat, N., Vrielinck, H. & Louwye, S. 2018. Taxonomic re-investigation and geochemical characterization of Reid's (1974) species of *Spiniferites* from holotype and topotype material. *Palynology* 42:93–110.
- Hall, T. A. 1999. BioEdit: A User-Friendly Biological Sequence Alignment Editor and Analysis Program for Windows 95/98/NT. *Nucl Acids Symposium Series* 41:95–8.
- Harland, R. 1983. Distribution maps of Recent dinoflagellate cysts in bottom sediments from the North-Atlantic Ocean and adjacent seas. *Palaeontology* 26:321–87.
- Harland, R., Nordberg, K. & Filipsson, H. L. 2006. Dinoflagellate cysts and hydrographical change in Gullmar Fjord, west coast of Sweden. *Sci. Total Environ.* 355:204–31.
- Head, M. J. 2007. Last Interglacial (Eemian) hydrographic conditions in the

- southwestern Baltic Sea based on dinoflagellate cysts from Ristinge Klint, Denmark. *Geological Magazine* 144:987–1013.
- Head, M. J., Mertens, K. N. & Fensome, R. A. 2023. Dual nomenclature in organic-walled dinoflagellate cysts I: concepts, methods and applications. *Palynology* 48:2290200.
- Head, M. J., Mertens, K. N. & Fensome, R. A. 2024. Dual nomenclature in organic-walled dinoflagellate cysts II: *Spiniferites elongatus* and *S. membranaceus*, and their equivalent non-fossil species *Gonyaulax ovum* comb. nov. and *G. lewisiae* sp. nov. *Palynology* 48:2300838.
- Huang, S., Mertens, K. N., Derrien, A., David, O., Shin, H. H., Li, Z., Cao, X., Cabrini, M., Klisarova, D & Gu, H. 2025. *Gonyaulax montresoriae* sp. nov. (Dinophyceae) from the Adriatic Sea produces predominantly yessotoxin. *Harmful Algae* 141:102761.
- Katoh, K. & Standley, D. M. 2013. MAFFT multiple sequence alignment software version 7: improvements in performance and usability. *Mol. Biol. Evol.* 30:772–80.
- Kofoed, C. A. 1911. Dinoflagellata of the San Diego region, IV. The genus *Gonyaulax* with notes on its skeletal morphology and a discussion of its generic and specific characters. *University of California Publication in Zoology* 8:187–286.
- Lewis, J., Rochon, A. & Harding, I. 1999. Preliminary observations of cyst-theca relationships in *Spiniferites ramosus* and *Spiniferites membranaceus* (Dinophyceae). *Grana* 38:113–24.

- Limoges, A., Londeix, L. & de Vernal, A. 2013. Organic-walled dinoflagellate cyst distribution in the Gulf of Mexico. *Mar. Micropaleontol.* 102:51–68.
- Limoges, A., Londeix, L., Mertens, K. N., Rochon, A., Pospelova, V., Cuéllar, T. & de Vernal, A. 2018. Identification key for Pliocene and Quaternary *Spiniferites* taxa bearing intergonal processes based on observations from estuarine and coastal environments. *Palynology* 42:72–88.
- Liu, D., Shi, Y., Di, B., Sun, Q., Wang, Y., Dong, Z. & Shao, H. 2012. The impact of different pollution sources on modern dinoflagellate cysts in Sishili Bay, Yellow Sea, China. *Mar. Micropaleontol.* 84:1–13.
- Marret, F., Bradley, L., de Vernal, A., Hardy, W., Kim, S.-Y., Mudie, P., Penaud, A., Pospelova, V., Price, A. M. & Radi, T. 2020. From bi-polar to regional distribution of modern dinoflagellate cysts, an overview of their biogeography. *Mar. Micropaleontol.* 159:101753.
- Matsuoka, K., 1985. Organic-walled dinoflagellate cysts from surface sediments of Nagasaki Bay and Senzaki Bay, West Japan. *Bull. Fac. Lib. Arts, Nagasaki Univ. Nat. Sci.*, 25:21–115.
- McMinn, A. 1991. Recent dinoflagellate cysts from estuaries on the central coast of New South Wales, Australia. *Micropaleontology* 37:269–87.
- Mertens, K. N., Aydin, H., Uzar, S., Takano, Y., Yamaguchi, A. & Matsuoka, K. 2015. Relationship between the dinoflagellate cyst *Spiniferites pachydermus* and *Gonyaulax ellegaardiae* sp. nov. from Izmir Bay, Turkey, and molecular characterization. *J. Phycol.* 51:560–73.

- Mertens, K. N. & Carbonell-Moore, C. 2018. Introduction to *Spiniferites* Mantell 1850 special issue. *Palynology* 42:1–9.
- Mertens, K. N., Van Nieuwenhove, N., Gurdebeke, P. R., Aydin, H., Bogus, K., Bringué, M., Dale, B., De Schepper, S., de Vernal, A. & Ellegaard, M. 2018. The dinoflagellate cyst genera *Achomosphaera* Evitt 1963 and *Spiniferites* Mantell 1850 in Pliocene to modern sediments: a summary of round table discussions. *Palynology* 42:10–44.
- Orlova, T. Y., Morozova, T. V., Gribble, K. E., Kulis, D. M. & Anderson, D. M. 2004. Dinoflagellate cysts in recent marine sediments from the east coast of Russia. *Bot. Mar.* 47:184–201.
- Pitcher, G. C., Foord, C. J., Macey, B. M., Mansfield, L., Mouton, A., Smith, M. E., Osmond, S. J. & van der Molen, L. 2019. Devastating farmed abalone mortalities attributed to yessotoxin-producing dinoflagellates. *Harmful Algae* 81:30–41.
- Posada, D. 2008. jModelTest: Phylogenetic Model Averaging. *Molecular Biology and Evolution* 25:1253–6.
- Pospelova, V., Chmura, G. L., Boothman, W. S. & Latimer, J. S. 2005. Spatial distribution of modern dinoflagellate cysts in polluted estuarine sediments from Buzzards Bay (Massachusetts, USA) embayments. *Mar. Ecol. Prog. Ser.* 292:23–40.
- Pospelova, V., de Vernal, A. & Pedersen, T. F. 2008. Distribution of dinoflagellate cysts in surface sediments from the northeastern Pacific Ocean (43–25 °N) in relation

- to sea-surface temperature, salinity, productivity and coastal upwelling. *Mar. Micropaleontol.* 68:21–48.
- Pospelova, V. & Kim, S.-J. 2010. Dinoflagellate cysts in recent estuarine sediments from aquaculture sites of southern South Korea. *Mar. Micropaleontol.* 76:37–51.
- Pospelova, V., Zonneveld, K. A., Heikkilä, M., Bringué, M., Price, A. M., Esenkulova, S. & Matsuoka, K. 2018. Seasonal, annual, and inter-annual *Spiniferites* cyst production: a review of sediment trap studies. *Palynology* 42:162–81.
- Reid, P. 1974. Gonyaulacacean dinoflagellate cysts from the British Isles. *Nova Hedwig* 25:579–637.
- Rhodes, L., McNabb, P., De Salas, M., Briggs, L., Beuzenberg, V. & Gladstone, M. 2006. Yessotoxin production by *Gonyaulax spinifera*. *Harmful Algae* 5:148–55.
- Riccardi, M., Guerrini, F., Roncarati, F., Milandri, A., Cangini, M., Pigozzi, S., Riccardi, E., Ceredi, A., Ciminiello, P. & Dell’Aversano, C. 2009. *Gonyaulax spinifera* from the Adriatic sea: Toxin production and phylogenetic analysis. *Harmful Algae* 8:279–90.
- Ronquist, F. & Huelsenbeck, J. P. 2003. MrBayes 3: Bayesian phylogenetic inference under mixed models. *Bioinformatics* 19:1572–4.
- Rosignol, M. 1964. Hystrichosphères du Quaternaire en Méditerranée orientale, dans les sédiments Pléistocènes et les boues marines actuelles. *Revue de micropaléontologie* 7:83–99.
- Ryther, J. H. & Guillard, R. R. L. 1962. Studies of marine planktonic diatoms: III. Some

- effects of temperature on respiration of five species. *Can. J. Microbiol.* 8:447–53.
- Saunders, G.W., Hill, D.R.A., Sexton, J.P. & Andersen, R.A. 1997. Small-subunit ribosomal RNA sequences from selected dinoflagellates: testing classical evolutionary hypotheses with molecular systematic methods. *Plant Syst. Evol.* (Suppl.) 11:237–59.
- Shin, H. H., Li, Z., Mertens, K. N., Yoo, Y. D., Youn, J. Y., Lee, M. & Gu, H. 2024. Morphology and molecular phylogeny of *Gonyaulax kunsanensis* sp. nov. (Gonyaulacales, Dinophyceae) from Korean coastal waters. *Bot. Mar.* <https://doi.org/10.1515/bot-2023-0106>.
- Silvestro, D. & Michalak, I. 2012. raxmlGUI: a graphical front-end for RAxML. *Org. Divers. Evol.* 12:335–7.
- Turland, N. J., Wiersema, J. H., Barrie, F. R., Greuter, W., Hawksworth, D., Herendeen, P. S., Knapp, S., Kusber, W.-H., Li, D.-Z. & Marhold, K. 2018. *International Code of Nomenclature for algae, fungi, and plants (Shenzhen Code) adopted by the Nineteenth International Botanical Congress Shenzhen, China, July 2017* [Regnum Vegetabile 159]. Koeltz Botanical Books, Oberreifenberg.
- Van Nieuwenhove, N., Potvin, É., Heikkilä, M., Pospelova, V., Mertens, K. N., Masure, E., Kucharska, M., Yang, E. J., Chomérat, N. & Zajaczkowski, M. 2018. Taxonomic revision of *Spiniferites elongatus* (the resting stage of *Gonyaulax elongata*) based on morphological and molecular analyses. *Palynology* 42:111–34.

- Vernette, C., Henry, N., Lecubin, J., de Vargas, C., Hingamp, P. & Lescot, M. 2021. The Ocean barcode atlas: A web service to explore the biodiversity and biogeography of marine organisms. *Mol. Ecol. Res.* 21:1347–58.
- Wall, D. 1965. Modern hystrichospheres and dinoflagellate cysts from the Woods Hole region. *Grana* 6:297–314.
- Wall, D. & Dale, B. 1966. "Living Fossils" in Western Atlantic Plankton. *Nature* 211:1025–6.
- Wang, N., Mertens, K. N., Krock, B., Luo, Z., Derrien, A., Pospelova, V., Liang, Y., Bilien, G., Smith, K. F., De Schepper, S., Wietkamp, S., Tillmann, U. & Gu, H. 2019. Cryptic speciation in *Protoceratium reticulatum* (Dinophyceae): Evidence from morphological, molecular and ecophysiological data. *Harmful Algae* 88:101610.
- Wang, Z., Matsuoka, K., Qi, Y. & Chen, J. 2004. Dinoflagellate cysts in recent sediments from Chinese coastal waters. *Mar. Ecol.* 25:289–311.
- Williams, G.L., Fensome, R.A., & MacRae, R.A., 2017. DINOFLAJ3. American Association of Stratigraphic Palynologists, Data Series no. 2.
- Zonneveld, K. A., Marret, F., Versteegh, G. J., Bogus, K., Bonnet, S., Bouimetarhan, I., Crouch, E., de Vernal, A., Elshanawany, R. & Edwards, L. 2013. Atlas of modern dinoflagellate cyst distribution based on 2405 data points. *Rev. Palaeobot. Palynol.* 191:1–197.

Figure legends

Fig. 1. Micrographs of *Gonyaulax carbonell-mooreae*. (a–e) Bright-field light microscopy. (f) Scanning electron microscopy. (a) A living cyst from Xiamen Bay yielding strain TIO717, showing the pronounced apical boss (arrow). (b) The same cyst as in A after hatching, showing the intergonal processes. (c) The same cyst in A after hatching, showing the cingular displacement. (d) The same cyst in A after hatching, showing the precingular archeopyle. (e) The living cyst of isolate HSN128 from the Bohai Sea. (f) An empty cyst from recent sediments of Xiamen Bay.

Scale bars = 20 μ m.

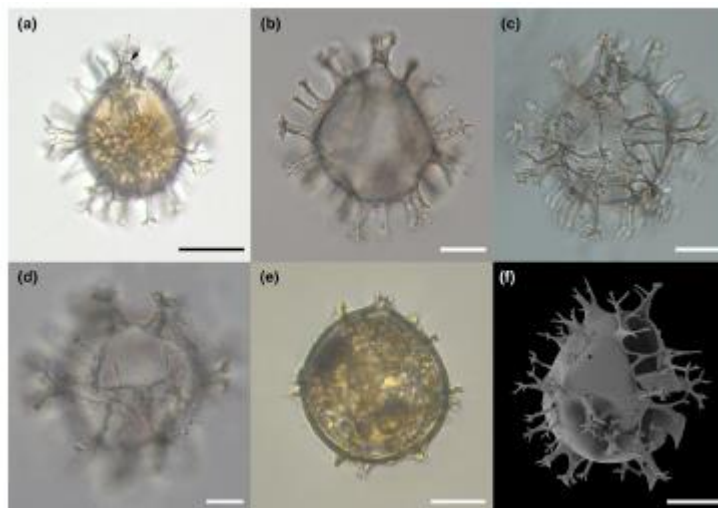


Fig. 2. Scanning electron micrographs of *Gonyaulax carbonell-mooreae* strain VINIF07. (a) Ventral view of a living cell, showing the pronounced horn and shoulders, and two antapical spines. (b) Ventral view of a living cell showing three apical plates, four precingular plates, and the anterior sulcal plate (Sa). (c) A broken cell showing six cingular plates (1c–6c). (d) Dorsal view of a cell showing two precingular plates (3''–4'') and two postcingular plates (*4'''–*5'''). (e) Antapical view of a cell showing five postcingular plates (*2'''–*6'''), one antapical plate (1''''), and two posterior intercalary plates (1p, 2p). (f) Ventral view showing the left anterior sulcal plate (Ssa), left posterior sulcal plate (Ssp), and posterior right sulcal plate (Sdp). Scale bars = 10 μ m.

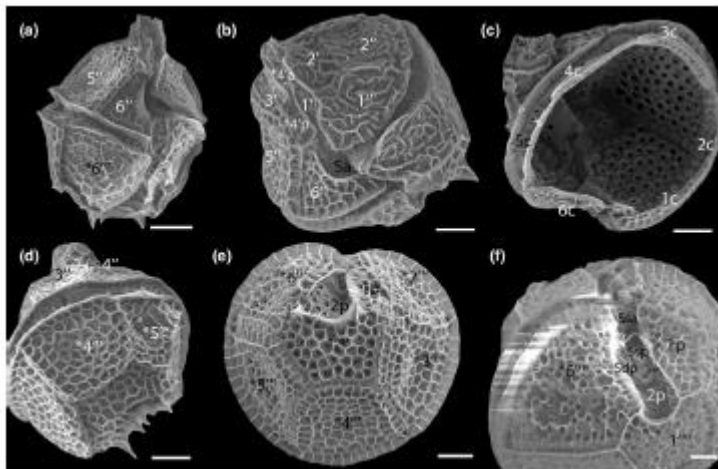


Fig. 3. Schematic drawing of *Gonyaulax carbonell-mooreae*. (a) Ventral view. (b) Dorsal view. (c) Antapical view. (d, e) Thecal reticulated ornamentation of *4''' and 1''', respectively.

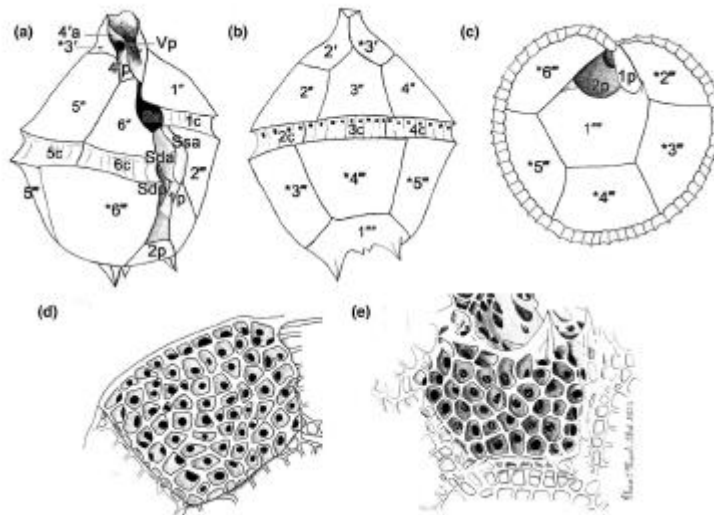


Fig. 4. Micrographs of *Gonyaulax kunsanensis*. (a–c) Bright-field light microscopy.

(d–i) Scanning electron microscopy. (a, b) A living cyst from strain TIO1274 showing the large antapical flange. (c) The same cyst as in A, showing the intergonal processes. (d) Cyst produced in culture of strain TIO219, showing the reduced archeopyle and fenestrate bases of processes (arrows). (e, f) Two cysts from Ningde, the East China Sea. (g–i) A living cyst from Xiamen Bay, showing the large antapical flange. Scale bars = 10 μm , except in (a–c) = 20 μm .

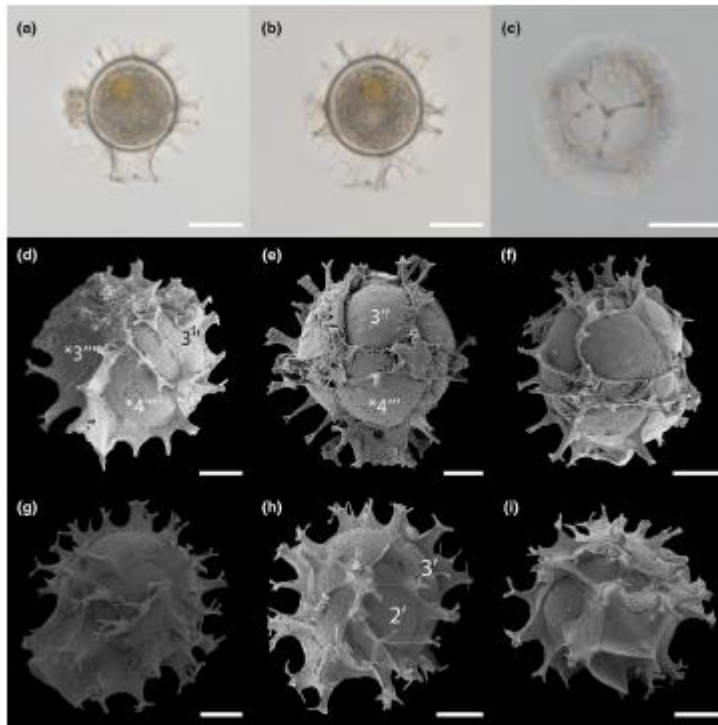


Fig. 5. Micrographs of *G. kunsanensis* strain TIO1221. (a–c) Bright-field light microscopy. (d–i) Scanning electron microscopy. (a) Ventral view of a living cell, showing the pronounced horn and shoulder on the right. (b) Ventral view of a living cell, showing chloroplast lobes. (c) SYBR Green-stained cell showing the elongated nucleus (N) in the hypocone. (d) Ventral view of a cell showing cingular displacement, two antapical spines, and the anterior sulcal plate (Sa). (e) Dorsal view of a cell showing two precingular plates (3''–4'') and two postcingular plates (*4'''–*5'''). (f) Apical view of a cell showing two apical plates (2', *3') and six precingular plates (1''–6''). (g) Apical view of a cell showing the apical pore complex (apc). (h) Antapical view of a cell showing five postcingular plates (*2'''–*6'''), one antapical plate (1'''), and two posterior intercalary plates (1p, 2p). (i) Ventral view showing the left anterior sulcal plate (Ssa), left posterior sulcal plate (Ssp), anterior right sulcal plate (Sda), and posterior right sulcal plate (Sdp). Scale bars = 5 μm , except in (a–c) = 10 μm .

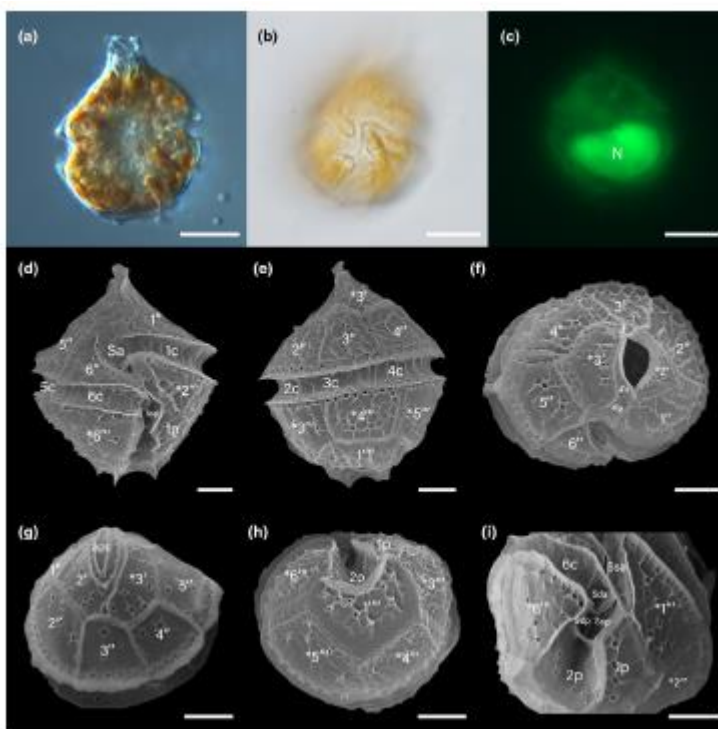


Fig. 6. Light micrographs of *Gonyaulax cf. lewisiae* isolate 18-652. (a) The empty cyst in mid focus, showing the antapical flange. (b) The same cyst in dorsal view, showing the archeopyle. (c) The same cyst in ventral view, showing the paracingulum and parasulcus. (d) The same cyst, showing the granular surface. (e) Germinated cell in mid focus, showing a shoulder on the right and a pronounced apical horn. (f, g) The same cell in ventral view, showing the cingular displacement and overhang. Scale bars = 20 μm , except in (e–g) = 10 μm .

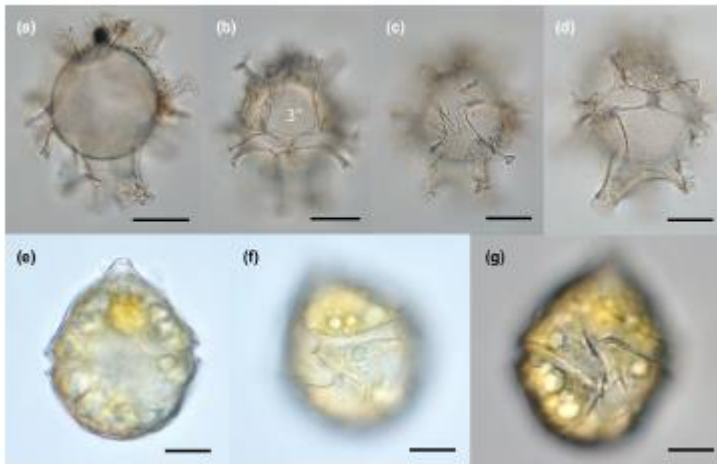


Fig. 7. Molecular phylogeny of *Gonyaulax* inferred from partial LSU rRNA gene sequences based on Bayesian inference (BI). *Adenoides eludens* (GenBank accession: LC002845) was used as the outgroup. New sequences are shown in bold red. Numbers at nodes represent Bayesian posterior probabilities and ML bootstrap values, asterisks (*) indicate maximal support (100% ML bootstrap support and 1.00 Bayesian posterior probabilities). Bootstrap values > 50% and posterior probabilities > 0.90 are shown. Branch lengths drawn to scale, with the scale bar indicating number of nucleotide substitutions per site.

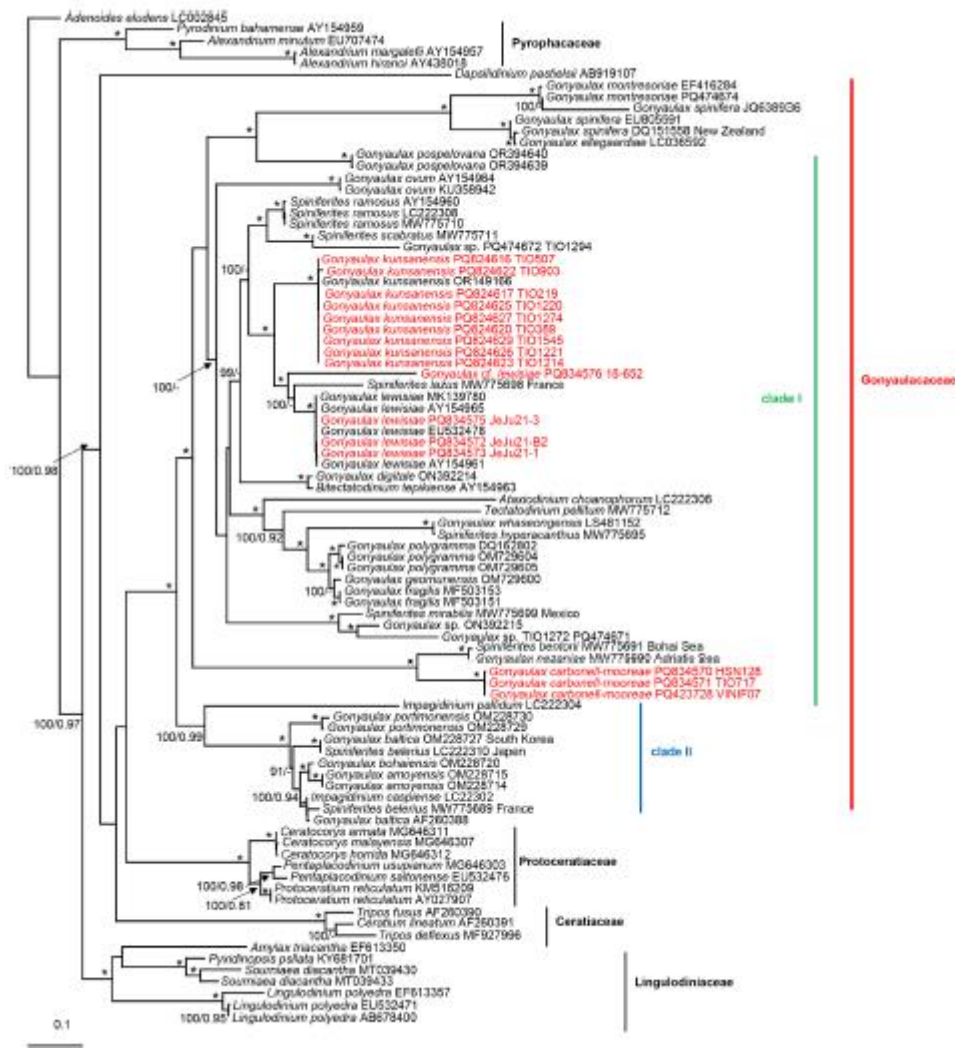


Fig. 8. Relative abundance of *Gonyaulax kunsanensis* (ASV71086) from the Tara Oceans 18S V4 metabarcoding data. Pink circle: 5–20 μm ; Purple circle: 20–180 μm .

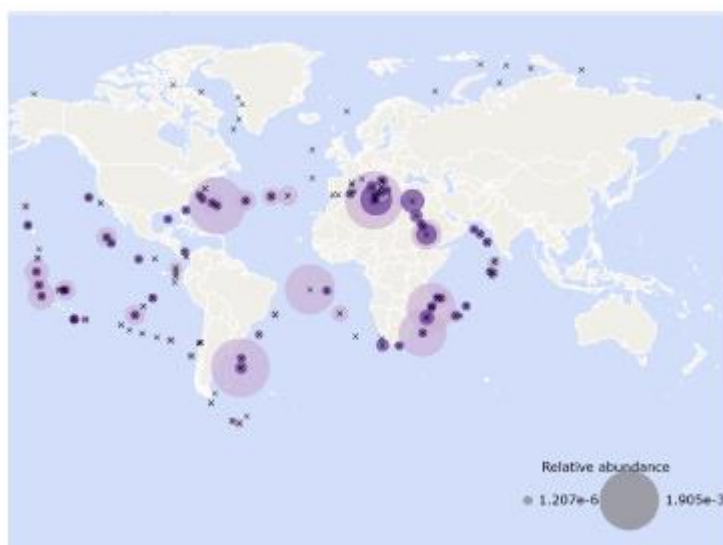


Table 1. *Gonyaulax* strains examined in the present study, including the collection locality, coordinates and collection date (NA: not available).

Species	Strains	Latitude (N)	Longitude (E)	Collection date	Collection locality	Origin	LSU/ITS
<i>G. kunsanensis</i>	TIO219	27°28'33"	121°03'53"	Jan. 6, 2016	Wenzhou, China	Cyst	PQ824617/-
<i>G. kunsanensis</i>	TIO220	27°28'33"	121°03'53"	Jan. 6, 2016	Wenzhou, China	Cyst	PQ824619/-
<i>G. kunsanensis</i>	TIO222	27°28'33"	121°03'53"	Jan. 6, 2016	Wenzhou, China	Cyst	PQ824618/-
<i>G. kunsanensis</i>	TIO389	22°35'55"	114°36'17"	Oct. 16, 2016	Daya Bay, China	Cyst	PQ824620/-
<i>G. kunsanensis</i>	TIO507	38°53'59"	122°49'32"	May 19, 2016	Dallan, China	Cyst	PQ824616/PQ834602
<i>G. kunsanensis</i>	TIO902	37°26'59"	121°34'19"	Sep. 3, 2016	Yantai, China	Cyst	PQ824621/PQ834603
<i>G. kunsanensis</i>	TIO903	37°26'59"	121°34'19"	Sep. 3, 2016	Yantai, China	Cyst	PQ824622/PQ834604
<i>G. kunsanensis</i>	TIO1214	36°00'09"	120°21'16"	Nov. 5, 2019	Qingdao, China	Cyst	PQ824623/-
<i>G. kunsanensis</i>	TIO1217	36°00'09"	120°21'17"	Nov. 5, 2019	Qingdao, China	Cyst	PQ824624/PQ834605
<i>G. kunsanensis</i>	TIO1220	36°00'09"	120°21'17"	Nov. 5, 2019	Qingdao, China	Cyst	PQ824625/-
<i>G. kunsanensis</i>	TIO1221	36°00'09"	120°21'17"	Nov. 5, 2019	Qingdao, China	Cyst	PQ824626/PQ834606
<i>G. kunsanensis</i>	TIO1223	25°32'54"	120°24'54"	Nov. 12, 2019	Taiwan Strait, China	Cyst	PQ836645/-
<i>G. kunsanensis</i>	TIO1274	24°31'30"	118°04'03"	Nov. 22, 2020	Xiamen Bay, China	Cyst	PQ824627/-
<i>G. kunsanensis</i>	TIO1506	24°25'39"	118°04'19"	Nov. 22, 2020	Xiamen Bay, China	Cyst	PQ824628/-
<i>G. kunsanensis</i>	TIO1538	26°31'53"	119°55'37"	June 4, 2022	Ningde, China	Cyst	PQ836646/-
<i>G. kunsanensis</i>	TIO1544	26°25'10"	119°54'25"	June 1, 2022	Ningde, China	Cyst	PQ836647/-
<i>G. kunsanensis</i>	TIO1545	26°23'11"	119°55'34"	May 31, 2022	Ningde, China	Cyst	PQ824629/-
<i>G. kunsanensis</i>	TIO1546	26°33'49"	120°05'18"	June 4, 2022	Ningde, China	Cyst	PQ836648/-
<i>G. kunsanensis</i>	TIO1547	26°31'55"	120°05'38"	June 4, 2022	Ningde, China	Cyst	PQ836649/-
<i>G. carbonell-mooreae</i>	TIO1717	24°35'33"	118°09'12"	Dec. 31, 2017	Xiamen Bay, China	Cyst	PQ834571/PQ834607
<i>G. carbonell-mooreae</i>	HSN128	38°37'56"	118°23'27"	Oct. 26, 2020	Bohai Sea, China	Cyst	PQ834570/-
<i>G. carbonell-mooreae</i>	VINIF07	16°33'11"	107°38'47"	May 28, 2022	Viet Nam	Cell	PQ423728/PQ4237254
<i>G. carbonell-mooreae</i>	VINIF08	16°33'11"	107°38'47"	May 28, 2022	Viet Nam	Cell	PQ423729/PQ4237255
<i>G. lewislae</i>	JeJu21-B2	33°13'16"	126°17'47"	July 23, 2021	Jeju, South Korea	Cell	PQ834572/-
<i>G. lewislae</i>	JeJu21-1	33°13'60"	126°22'33"	July 23, 2021	Jeju, South Korea	Cell	PQ834573/-
<i>G. lewislae</i>	JeJu21-3	33°13'39"	126°28'36"	July 23, 2021	Jeju, South Korea	Cell	PQ834575/-
<i>G. cf. lewislae</i>	18-652	47°50'00"	-3°56'60"	May 28, 2018	Concarneau large, France	Cyst	PQ834576/-

Table 2. Comparison of cyst morphology of *G. kunsanensis* and *Gonyaulax carbonell-mooreae* with related *Spiniferites* species. NA: not available

Species	<i>G. kunsanensis</i>	<i>S. membranaceus</i>	<i>S. mirabilis</i> subsp. <i>mirabilis</i>	<i>G. carbonell-mooreae</i>	<i>S. bullatus</i>	<i>S. bentorii</i>	<i>S. cf. bentorii</i>
Strain/isolate	TIO1221 etc	NA	20-188	TIO717, HSN128	NA	NA	WN20-WN22
Cyst shape	Spherical	Circular to ovoid	Ovoid	Pear-shaped	Pear-shaped	Pear-shaped	Pear-shaped
Cyst length (µm)	31.8-37.5	36-44	35	55.0-70.2	66-82	60-73	49.8-63.9
Cyst width (µm)		34-42	30	43.0-65.7	60-77	45-63	43.5-52.8
Apical boss	None	Clear	Clear	Pronounced	Pronounced	Pronounced	Pronounced
Antapical flanges	Present, 4 processes	Present, 2 processes	Present, 5-7 processes	Absent	Absent	Absent	Absent
Processes	1-3 Intergonal processes	Exclusively gonial	<3 Intergonal processes	<3 Intergonal processes	<3 Intergonal processes	Intergonal processes occasional	<3 Intergonal processes
Perforations at the process base	Occasionally	None	NA	None	NA	Rare	None
Process length (µm)	6.5-10.8	12-17	6.7-8.3	4.5-15.7	8-13	15-20, 25 for the antapical processes	4.2-7.3
Cingulum displacement	1.5	2.0	2.0	1.0	1.0	None	3.0
Cyst wall ornamentation	Smooth to microgranulate	Granulated	Microgranulate	Smooth	Smooth	Microgranulate	Finely granulated
Archeopyle	Reduced	Reduced	Reduced	Not reduced	Not reduced	Reduced	Reduced
References	Present study, Shin et al. (2024)	Reid (1974), Gurdebeke et al. (2018)	Limoges et al. (2018), Gu et al. (2021)	Present study	Bellstein (1994)	Rosignol (1964), Limoges et al. (2018)	Gu et al. (2021)

Table 3. Comparisons of motile cell features of *G. kunsanensis* and related species

Character	<i>G. carbonell-mooreae</i>	<i>G. diegensis</i>	<i>G. spinifera</i>	<i>G. kunsanensis</i>	<i>G. digitale</i>	<i>G. nezaniae</i>	<i>G. ellegaardiae</i>	<i>G. lewisiae</i>
Strain/isolate	VINIF07	NA	TIO701	LMBE-V570	NA	Pantan	NA	NA
Length (µm)	51.8-57.1	60-100	27-41	33-47	50-75	37-68	31-43	30-48
Width (µm)	42.3-60.0	45-82	22-33	26-37	34-50	33-52	24-35	23-43
Shoulders	Pronounced in the right	Pronounced in the right	Pronounced	Pronounced in the right	Intermediate	Intermediate	Pronounced in the left	Intermediate
Reticulation	Pronounced	Pronounced	Pronounced	Intermediate	Pronounced	Pronounced	Pronounced	Strongly
Pores	Many	Many	Intermediate	Intermediate	Many	Intermediate	Many	Intermediate to many
Cingulum displacement	1.0	6.0	1.0	3.0	2.0-2.5	3.0	2.5-3.0	2.5-4.0
Cingulum overhang	0	0-1.5	0.5-1.0	1.0	1.0-1.3	1.7	2.0	2.0-4.0
Angle	10°	10°	15°	20°	13-18°	20°	30°	20-29°
Antapical spines	2, equal	2-3	2	2	2	2	4, finned	2-4, one prominent, finned sometimes
Length of spines (µm)	4.2-5.4	1.0-3.0	1.2-5.1	3-5	3-10	2-11	5.7-6.0	2-4
Form of sulcus	Not abruptly widened	Abruptly widened	Not abruptly widened	Abruptly widened	Abruptly widened	Abruptly widened	Not abruptly widened	Not abruptly widened
Apical horn, girdle widths in length	Prominent, 1.5	Prominent, 3.0-6.0	Prominent, 2.0	Prominent, 1.6	Prominent, 2.0	Prominent, 1.3-2.0	Not prominent, 1.0	Not prominent, 1.0
Ventral pore	Present	Present	Present	Present	Present	Present	Present	Present
References	Present study	Kotold (1911)	Gu et al. (2021)	Shin et al. (2024)	Kotold (1911), Gu et al. (2021)	Gu et al. (2021)	Merlens et al. (2015)	Lewis et al. (1999)

Supplementary Materials

Fig. S1. Light micrographs (LM) of cells of *Gonyaulax carbonell-mooreae* strain

TIO717. (A–C) Dorsal view, different focus showing the reticulations.

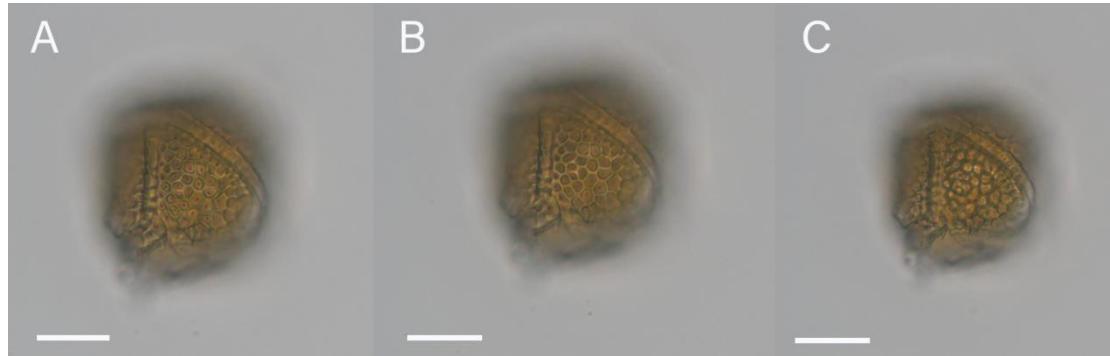


Fig. S2. The occurrence of *Gonyaulax kunsanensis* (ASV71086) at different depths and corresponding temperatures from the Tara Oceans 18S V4 metabarcoding data. SRF: surface ocean; DCM: deep chlorophyll maximum; ZZZ: marine water layer; MES: mesopelagic zone; MIX: marine epipelagic mixed layer.

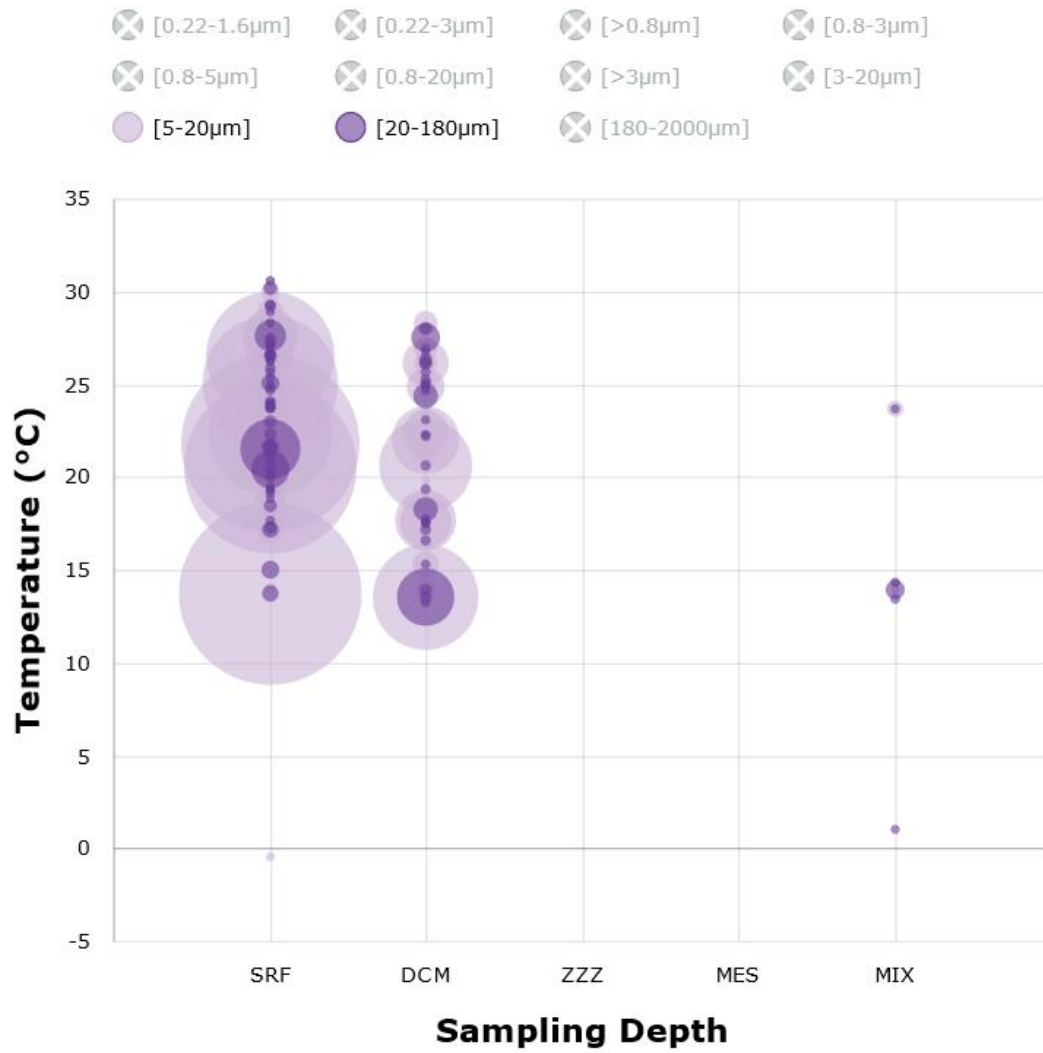


Fig. S3 Relative abundance of *Gonyaulax lewisiae* (ASV76747) from the Tara Oceans 18S V4 metabarcoding data.

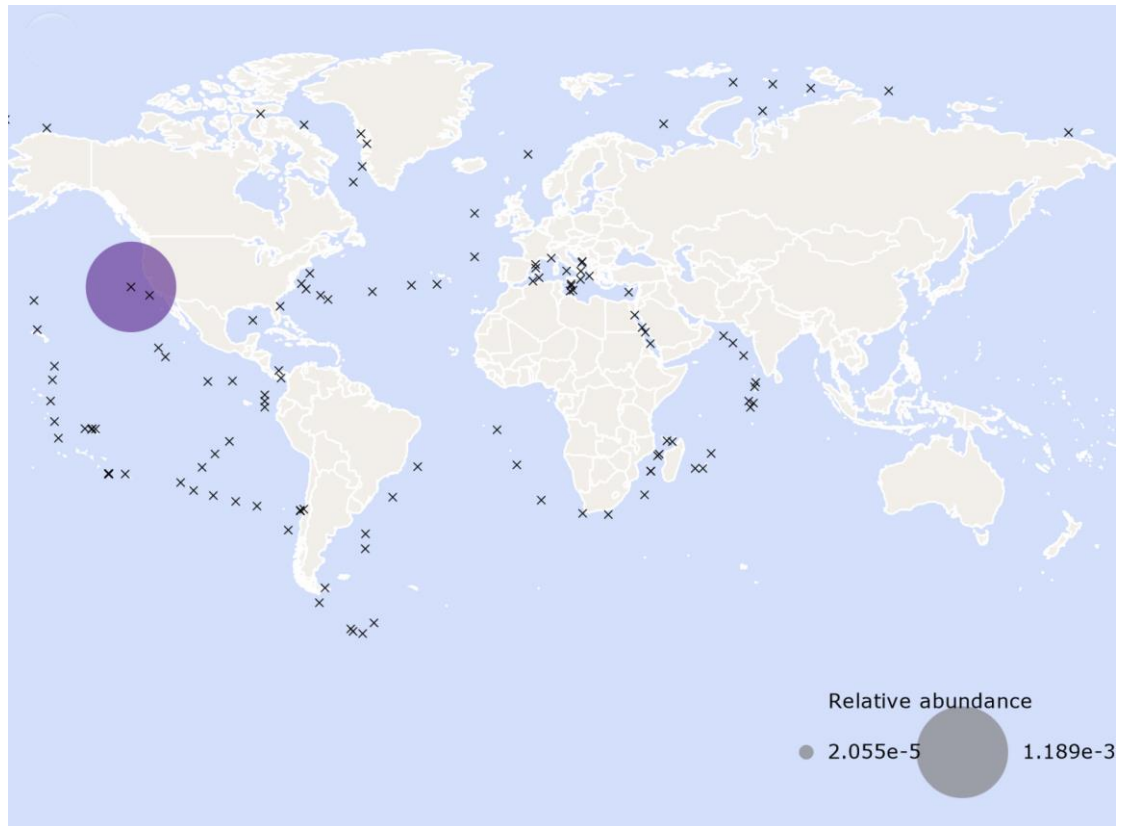


Fig. S4. The occurrence of *Gonyaulax lewisiae* (ASV76747) at different depths and corresponding temperatures from the Tara Oceans 18S V4 metabarcoding data. DCM: deep chlorophyll maximum; SRF: surface ocean.

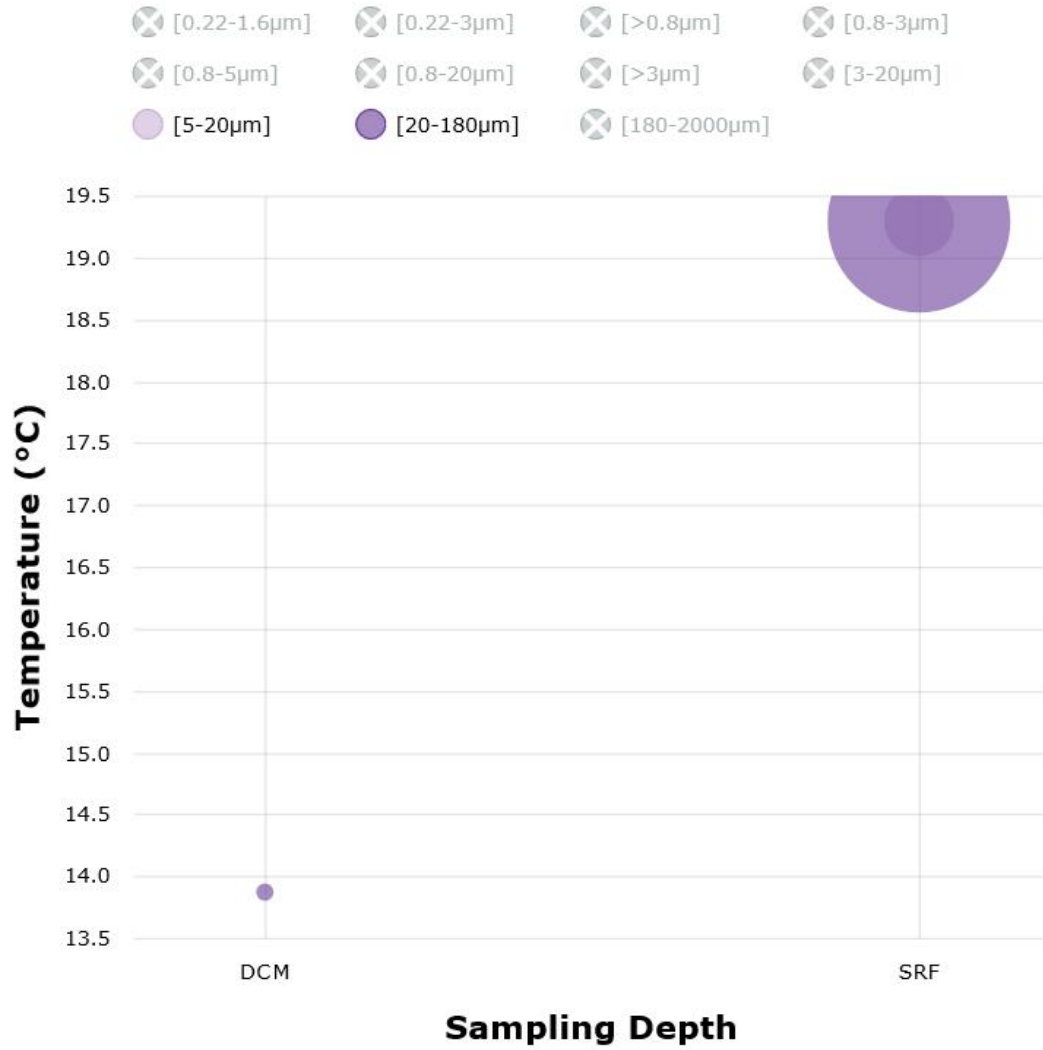


Table S1 Mass transitions of the selected reaction monitoring (SRM) LC-MS/MS experiments and their respective YTX designations cited in Sala-Pérez et al. (2016). All compounds and entries refer to original numbering in Miles et al. (2005).

Q1 mass (<i>m/z</i>)	Q3 mass (<i>m/z</i>)	YTX
991	911	Compounds 17–19
1047	967	41-keto-YTX/40-epi-41-keto-YTX/41-keto-YTX-enone (compounds 6,7,8)
1049	969	Undescribed
1061	981	Entries 21, 22
1085	1005	Compound 16
1101	1021	Nor-YTX (compound 5)
1117	1037	Entry 17
1131	1051	Undescribed
1141	1061	YTX, entries (32-35)
1143	1063	Entry 37
1155	1075	41a-homo-YTX (compound 5)
1157	1077	45-OH-YTX (compound 2)
1159	1079	Entry 45
1169	1089	9-Me-41a-homo-YTX (compound 10)
1171	1091	Undescribed
1173	1193	Entry 50
1175	1095	44,55-dihydroxy-YTX
1187	1107	Carboxy-homo-YTX
1189	1109	Entry 61
1195	1115	Undescribed
1203	1123	Entry 67
1273	1193	Entry 92
1290	1210	Entry 77
1304	1224	Compound 12